Monitoring subwavelength grating structures for vertical-cavity surface-emitting laser applications by spectroscopic ellipsometry

Emeric Balogh, Peter Basa,[a] Attila Suto, Benjamin Powell, Anna Bölcskei-Molnár, and Szilvia Biró
Semilab Semiconductor Physics Laboratory Co. Ltd., Budapest H-1117, Hungary

(Received 31 July 2019; accepted 6 November 2019; published 22 November 2019)

GaAs based vertical cavity surface emitting lasers (VCSELs) have one of the fastest growing markets due to their numerous applications in imaging technology, optical sensors, and interconnects. Stable, single-mode operation of these laser diodes is often achieved by forming subwavelength structures on the surface of the GaAs semiconductor. Quick and preferably noncontact inspection of the formed nanostructures is desired during the fabrication process. Nanostructure characterization by spectral ellipsometry-based metrologies has become an indispensable tool in the semiconductor industry. An advanced method of ellipsometry is the application of Mueller-matrix ellipsometry, which enables the characterization of structure details difficult to measure or not reachable by using standard ellipsometry measurements. In this paper, the authors present the results of nanostructure characterization by model-based dimension metrology using spectral ellipsometry and Mueller-matrix spectral ellipsometry of line gratings formed on GaAs substrates during the process of VCSEL fabrication. *Published by the AVS.* https://doi.org/10.1116/1.5122771

I. INTRODUCTION

GaAs based vertical cavity surface emitting lasers (VCSELs) have been widely studied recently due to their numerous demonstrated and prospective applications. They have many advantageous properties like narrow emission bandwidth, which enables very sensitive time of flight detection with applications in imaging and depth sensors, and they are even used in atomic clocks.[1,2] Another outstanding feature is the quick response time to driving current modulations, which makes them a very promising light source in high-speed optical communication.[3,4] Many of these applications demand stable, single-mode operation of VCSEL devices. In the case of GaAs VCSELs, laser emission can occur along both the ⟨100⟩ and ⟨010⟩ crystalline planes.[5] Single-mode operation can be achieved by forming subwavelength gratings on the surface of the semiconductor to suppress emission in modes perpendicular to the grating lines.[6] This is a proven, efficient method of mode suppression and is already applied in mass production. Preparation of these subwavelength gratings requires cost-efficient, yet industry level quality method which in most cases is realized by nanoimprinting.[7] Monitoring of the parameters of the imprinted gratings is necessary for efficient process control. There are two main types of metrologies currently in use which are capable of producing accurate and fast measurement results required to maintain high throughput of VCSEL production lines: automatized atomic force microscopy (AFM) and model-based dimension (MBD) characterization metrology.

In this contribution, we present MBD metrology based on spectral ellipsometry (SE-MBD) and on Mueller-matrix spectral ellipsometry (MM-MBD), measurement data of real-life product wafers, and MBD analysis of the measurements. We compare the two methods and highlight the performance and potential advantages and disadvantages of each.

The paper is organized as follows: in Sec. II, we present the sample fabrication process and details of the measurement apparatus and describe ellipsometry quantities essential for the understanding of the result. In Sec. III, we provide a brief theoretical description of ellipsometry-based MBD models. In Sec. IV, measurement results are described, and we conclude our results in Sec. V.

II. SAMPLE FABRICATION AND MEASUREMENT TECHNIQUES

A. Sample fabrication

During the fabrication of the VCSEL devices, GaAs wafers are used and coated with SiO_2 using the solgel method. The refractive index of the material deposited with the solgel method can be slightly different from the literature values of SiO_2; therefore, during the discussions in this paper, we are going to refer to the material simply as SolGel. Then, patterning of the SolGel surface is done by nanoimprinting. After the formation of the grating in the SolGel coating, grating lines in the GaAs substrate are formed using the reactive ion etching method. During these processes, some uncertainty by the imprinting process is introduced and therefore the orientation of the grating lines inside the sample may shift by a few degrees. This grating angle orientation and uncertainty has to be accounted for by any metrology to achieve reliable results of structure parameters and grating period, and it is especially important in SE-based metrology of nanogratings for reasons discussed in Secs. II B and II C.

B. Spectral ellipsometry

Samples were measured with the spectral ellipsometry tool (Semilab SE-2000) capable of SE measurement in the

Note: This paper is part of the Conference Collection: 8th International Conference on Spectroscopic Ellipsometry 2019, ICSE.
[a]Electronic mail: peter.basa@semilab.hu

region of 193–2500 nm. The spectral region needed to accurately characterize the structure depends on the sample; in general, we have used data in the region of 250–550 nm, with an incidence angle of 75°. This restricted spectral range was found to be a good compromise between precision and model computation time for this application. The same ellipsometry tool was used for the measurements of the 15 element Mueller matrix, described in Sec. II C.

In spectral ellipsometry measurement, light incident on a sample is interacting with the material and reflected toward the detector. The relative amplitudes and phases of s and p polarized waves are varying during the reflection, transforming the incident (usually linearly polarized) light into the elliptically polarized one. Let us denote the amplitudes of s and p polarization light waves incident on a sample as E_s^i and E_p^i, respectively. In the same manner, we define the reflected light amplitudes E_s^r and E_p^r.

The complex reflection coefficients are defined as $r_s = E_s^r/E_s^i$ and $r_p = E_p^r/E_p^i$. In spectral ellipsometry, the ratio ρ of the reflection coefficients is measured,[8] which is a complex quantity. The ellipsometric quantities Ψ and Δ are related to ρ as

$$\rho \equiv \tan(\Psi)\exp(-i\Delta) = \frac{r_p}{r_s}, \quad (1)$$

where r_p and r_s describe the complex reflection coefficients for p- and s-polarized waves, respectively. Equation (1) is complete only in cases when p- and s-polarized waves can be treated independently during the interaction of light with the sample. This is the case for isotropic samples and also for samples showing optical anisotropy, when the anisotropy axis is normal to the surface of the sample.[9]

Subwavelength gratings are known to show optical anisotropic behavior (different optical properties parallel and perpendicular to the grating lines), which is sometimes termed geometrical anisotropy, for the reason that it is linked to the geometric properties of the subwavelength (quasi-)periodic features of the sample. Gratings with periodicity comparable to the wavelength of incident light may exhibit several types of resonance phenomena, known as Wood's anomalies.[10,11] The signatures of these resonances are also visible in ellipsometry measurements. The grating angle has a strong effect on the measured ellipsometry spectra, and extra care must be taken when analyzing the data of such samples.

In general case, when the anisotropy axes enclose an arbitrary angle with the plane of incidence, the sample rotates the incident polarization, generating reflected p polarized light from the incident s-polarized waves, and the other way around as well. Then, the interaction can be described by the following equation:[8]

$$\begin{bmatrix} E_p^r \\ E_s^r \end{bmatrix} = \begin{bmatrix} r_{pp} & r_{ps} \\ r_{sp} & r_{ss} \end{bmatrix} \begin{bmatrix} E_p^i \\ E_s^i \end{bmatrix}, \quad (2)$$

where r_{ps} and r_{sp} describe the cross-terms, characteristic of anisotropic samples, which strongly depend on the enclosed angles between the anisotropy axes and the plane of incidence. The 2 by 2 matrix in Eq. (2) is often referred to as the Jones matrix and can accurately describe nondepolarizing anisotropic samples. The normalized Jones matrix of a sample is measured in generalized ellipsometry.

When using SE measurement in the case of anisotropic samples, the measured quantities depend on all four terms of the Jones matrix. The strong parameter correlation between structure parameters and grating angle makes it difficult or even impossible to accurately characterize samples from a single SE measurement if the orientation of grating lines is uncertain. One of the solutions is to align the samples prior to SE measurement based on an independent measurement capable of accurate grating angle characterization or to make multiple SE measurements by rotating the samples in the azimuthal direction. Both of these methods require a more complex mechanical hardware and increase total measurement time and are, therefore, not desirable in a production line.

C. Mueller-matrix ellipsometry

Another possibility to characterize the anisotropy of the samples is by using Mueller-matrix spectral ellipsometry. In this case, the Mueller matrix is used to determine the grating line orientation and structure parameters from a single measurement. This measurement technique is an advanced method of spectral ellipsometry, designed specifically for the purpose of measuring samples showing optical anisotropy. The Mueller matrix is a 4 by 4 matrix describing the transformation of the Stokes vector of light interacting with a material, in our case, the sample.

The four component Stokes vector completely describes the polarization state of light. The Stokes vector is described as $S = [I_s + I_p, \quad I_s - I_p, \quad I_{+45^\circ} - I_{-45^\circ}, \quad I_R - I_L]^T$, where I_s and I_p are the light intensities in s and p polarizations, I_{+45° and I_{-45° are the intensities of polarization components oriented at ±45°, and I_R and I_L are the intensities of left and right circular components of the wave. The benefit of using Stokes vectors for describing light polarization is that when the last three Stokes vectors are plotted in a spherical coordinate system, then the resulted sphere (the so-called Poincaré sphere) unambiguously shows all possible polarization states of light. In this case, even the partial depolarization (uncertain polarization state) can be described by an extended surface on the Poincaré sphere, instead of the pointlike state of perfectly polarized and unique vector.

Interaction of light with the sample (or an optical element) transforms the Stokes vector of incident light S^i; this transformation can be described by the MM of the interaction,

$$S^r = \mathrm{MM}\, S^i = \begin{bmatrix} mm_{11} & mm_{12} & mm_{13} & mm_{14} \\ mm_{21} & mm_{22} & mm_{23} & mm_{24} \\ mm_{31} & mm_{32} & mm_{33} & mm_{34} \\ mm_{41} & mm_{42} & mm_{43} & mm_{44} \end{bmatrix} S^i. \quad (3)$$

Measured Mueller matrices are most often normalized to the total reflected light intensity, which is the first element of the matrix (mm_{11}). Normalized, nondepolarizing Mueller matrices (although contain 15 elements with data) describe a total of six independent quantities for each wavelength, as opposed to only two that are measured with SE. The four additional quantities are related to the anisotropic properties of the sample. Depolarizing Mueller matrices contain additional information related to the depolarization properties of the sample. If the sample is not depolarizing the incident light, the MM can be calculated from the elements of the Jones matrix according to the following equation:

$$\mathrm{MM}=\begin{bmatrix} \frac{1}{2}\left(|r_{pp}|^2+|r_{sp}|^2+|r_{ps}|^2+|r_{ss}|^2\right) & \frac{1}{2}\left(|r_{pp}|^2+|r_{sp}|^2-|r_{ps}|^2-|r_{ss}|^2\right) & \mathrm{Re}(r_{pp}r_{ps}^*+r_{sp}r_{ss}^*) & \mathrm{Im}(r_{pp}r_{ps}^*+r_{sp}r_{ss}^*) \\ \frac{1}{2}\left(|r_{pp}|^2-|r_{sp}|^2+|r_{ps}|^2-|r_{ss}|^2\right) & \frac{1}{2}\left(|r_{pp}|^2-|r_{sp}|^2-|r_{ps}|^2+|r_{ss}|^2\right) & \mathrm{Re}(r_{pp}r_{ps}^*-r_{sp}r_{ss}^*) & \mathrm{Im}(r_{pp}r_{ps}^*-r_{sp}r_{ss}^*) \\ \mathrm{Re}(r_{pp}r_{sp}^*+r_{ps}r_{ss}^*) & \mathrm{Re}(r_{pp}r_{sp}^*-r_{ps}r_{ss}^*) & \mathrm{Re}(r_{pp}r_{ss}^*+r_{ps}r_{sp}^*) & \mathrm{Im}(r_{pp}r_{ss}^*-r_{ps}r_{sp}^*) \\ -\mathrm{Im}(r_{pp}r_{sp}^*+r_{ps}r_{ss}^*) & -\mathrm{Im}(r_{pp}r_{sp}^*-r_{ps}r_{ss}^*) & -\mathrm{Im}(r_{pp}r_{ss}^*+r_{ps}r_{sp}^*) & \mathrm{Re}(r_{pp}r_{ss}^*-r_{ps}r_{sp}^*) \end{bmatrix}, \tag{4}$$

where Re and Im represent the real and imaginary parts of the enclosed complex quantities. Normalizing the above matrix by m_{11} produces the 15 element MM that is usually measured with Mueller-matrix spectral ellipsometry. In the case of depolarizing samples, MM measurements can still be used, however, depending on the degree of depolarization; additional care must be taken to ensure the accuracy of the model in regression analysis.[12,13]

III. MODELING

SE-MBD and MM-MBD metrologies, in their traditional form, are model-based approaches used to characterize samples with periodically repeating structures along one or two dimensions. They require accurate modeling of the light-matter interaction to calculate the ellipsometry quantities produced in the measurement. Regression analysis is then used to refine the model to the point when the quantities calculated from the model fit the relevant quantities measured. This is an iterative method, which involves refining the model parameters and evaluating the model in each step of the fitting procedure. In this section, the modeling tools used in this metrology are briefly described.

Quantitatively accurate modeling of the light-matter interaction is required. This can be done computationally efficiently with rigorous coupled wave analysis (also called the Fourier Modal method), which was introduced by Moharam and Gaylord in the 1980s,[14] with an improved version published later by the same authors.[15,16] In this method, the periodic nature of the structure is accounted for, by expanding into Fourier series along one period for both the electric field and the spatial variation of the dielectric constant. Then, a set of coupled equations are solved for the Fourier components. Multilayer structures and structures with shapes which have tilted or curved sidewalls require a vertical slicing of the shape into thin layers.[16] The set of equations are then solved for each of the individual layers, and finally they are combined into the full transfer matrix of the complete structure enabling the calculation of the reflected and transmitted complex field amplitudes for all diffraction orders considered in the spatial Fourier expansion.[16]

Calculating the reflection from the modeled periodic structure for s and p polarized incident waves enables the calculation of all the components of the matrix in Eq. (2) for all diffraction orders. The model can be further simplified if additional symmetry relations are assumed. This is the case for 1D gratings in planar incidence, i.e., when the grating lines are exactly perpendicular to the plane of incidence. In this case, the fields of s and p polarizations can be calculated independently. The cross-terms [the off-diagonal elements in Eq. (2)] are zero; hence, only two complex quantities are calculated in this model (r_{pp} and r_{ss}), and two independent ellipsometric quantities can be derived. The general case—when the grating lines enclose an arbitrary angle with the plane of incidence—is called conical incidence, where the complete Jones matrix and six independent ellipsometric quantities can be calculated. With our algorithm, the calculation time is about a factor of eight shorter for the case of planar incidence than for the case of conical incidence, with all other parameters unchanged.

The time required to obtain the solution depends on the method used for matrix inversion. We use the basic algorithm as described by Dhoedt,[17] a commercial linear algebra package, and thread parallelization. For the models presented here, the planar incidence calculation was fast enough to obtain a solution within a few seconds on a normal consumer PC with four processor cores, when fitting the measurement at 60 separate wavelengths, or generate a library of tens of thousands of parameter combinations on the same PC in a few hours.

IV. RESULTS AND DISCUSSION

A. SE-MBD measurement of samples

During the process of the grating imprinting for VCSEL fabrication, there are two stages where MBD metrology is used: after the imprinting of the grating into the SolGel layer and after the dry-etching, during which the grating is formed in the GaAs substrate. For accurate refractive index data, the SolGel coating was characterized using spectral ellipsometry on a nonimprinted sample measured at three angles of incidence. The Sellmeier dispersion law was used to model the optical properties of the SolGel coating producing excellent fit quality and yielding a refractive index of 1.438 at

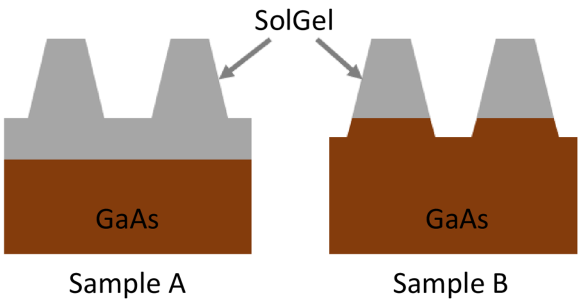

FIG. 1. Schematic of the sample structure of the two samples analyzed throughout this paper. *SolGel* represents SiO_2 coated on the substrate using the solgel method.

632.8 nm wavelength. In production of VCSELs, the most important quantities of the grating lines are the pitch of the grating, the depth of the trenches and the duty cycle, or the middle-CD (MCD), which is the width of the grating lines at half height of the trench.

After the imprinting process, when the grating in SolGel is formed, a residual layer may still remain on the bottom of the trenches. The structure of one of the preproduction wafers measured with SE-MBD shows such an incomplete etching (*sample A* in Fig. 1). SE-MBD measurement is capable of measuring not only the structure parameters of the grating itself but also the thickness of the residual layers below the grating. In this case, the SE-MBD can easily detect and characterize a 20 nm thick layer of SolGel thin films at the bottom of the trenches. Measured and fitted spectra are shown in Fig. 2, showing good agreement between model and measurement throughout the whole spectral region. During the fitting procedure, five floating parameters were used: the pitch, the residual thickness, the grid depth, and the width of the grid lines at the top and bottom of the grating walls. The parameters describing the width of the walls at the bottom of the trenches and the grid depth showed the strongest correlation of 0.84.

TABLE I. SE-MBD and AFM measurement results of sample A. MCD is the width of the SolGel grid lines at the middle height of the trench. Static repeatability values are below 0.2% (1 sigma) for all parameters except the residual thickness, in which case it is 0.8%.

	Pitch (nm)	Residual thickness (nm)	Grid depth (nm)	MCD (nm)
SE-MBD	143.6	19.6	88.9	63.7
AFM	141.9	—	89.6	80.3

In Table I, the results of the SE-MBD measurement and manual AFM measurements are compared (Vecco Dimension 3000 AFM) for sample A, showing good agreement for depth and pitch. Static reproducibility of the SE-MBD measurement was better than 0.2% in the case of all important parameters. In the case of the MCD, the curvature of the tip of the AFM needle may alter the result of the AFM measurement, which could possibly explain the discrepancy between SE-MBD and AFM measurement results.

After the dry-etching process when the grating in the GaAs is formed, some residual SolGel grating on top of the GaAs grating may remain as illustrated for *sample B* in Fig. 1. The analyzed preproduction sample shows an extreme example of this. SE-MBD measurement and fit results are shown in Fig. 3. In the case of such structures, SE-MBD is capable of detecting the depth of the GaAs grating and the residual SolGel grating separately. Results of SE-MBD and AFM measurements are summarized in Table II.

The depth of the GaAs grating is very small due to the incomplete etching of the preproduction wafers. Nonetheless, the total grid depth measured with SE-MBD metrology agrees well with the AFM measurements of the sample.

The SE-MBD measurements described above presumes that the angle of the grating line is known prior to the analysis. This can be ensured by rotating the sample in the azimuthal direction and taking multiple measurements. In Figs. 2 and 3,

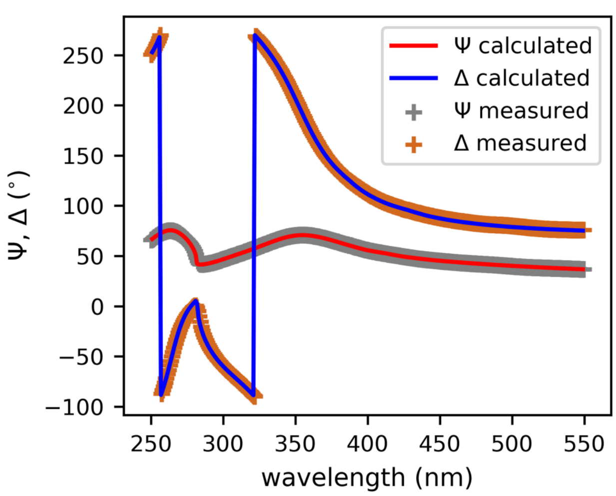

FIG. 2. Measurement and fitted ellipsometry spectra of *sample A* at planar incidence. Measurements and calculations were done at an angle of incidence of 75°.

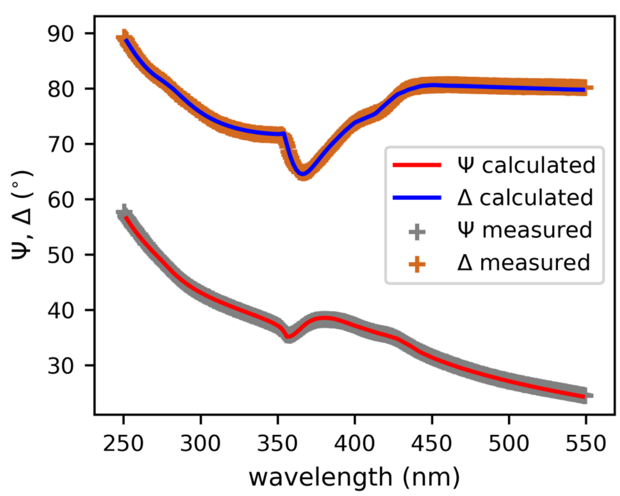

FIG. 3. Measurement and fitted ellipsometry spectra of *sample B* at planar incidence. Measurements and calculations were done at an angle of incidence of 75°.

TABLE II. SE-MBD and AFM measurement results for sample B. MCD is the width of the grid lines at the middle height of the trench. Repeatability of the results was better than 0.23% (1 sigma) for pitch, depth, and MCD. In the case of the GaAs etch depth, the repeatability in terms of standard deviation was found to be 0.023 nm.

	Pitch (nm)	Total depth (nm)	GaAs depth (nm)	MCD (nm)
SE-MBD	180.4	64.9	1.4	79.2
AFM	177.7	65.4	—	86.1

the signature peaks of Rayleigh–Wood anomalies are observed around 275 and 355 nm wavelengths, respectively. The azimuthal rotation produces a shift in the position of these signature peaks, which reach extrema at the orientations where the grating lines are perpendicular or parallel to the plane of incidence. This effect can be used to deduce the grating line

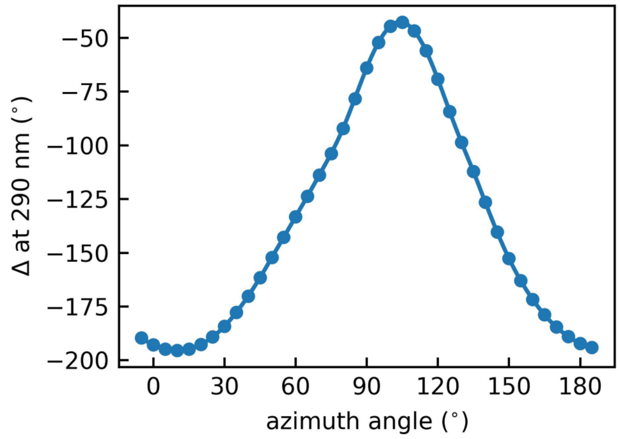

FIG. 4. Azimuthal rotation scan of sample A. Δ values at a wavelength of 290 nm are shown, illustrating the effect of the Rayleigh–Wood resonance peak shift. Azimuthal angles are shown with respect to a characteristic orientation of the wafer.

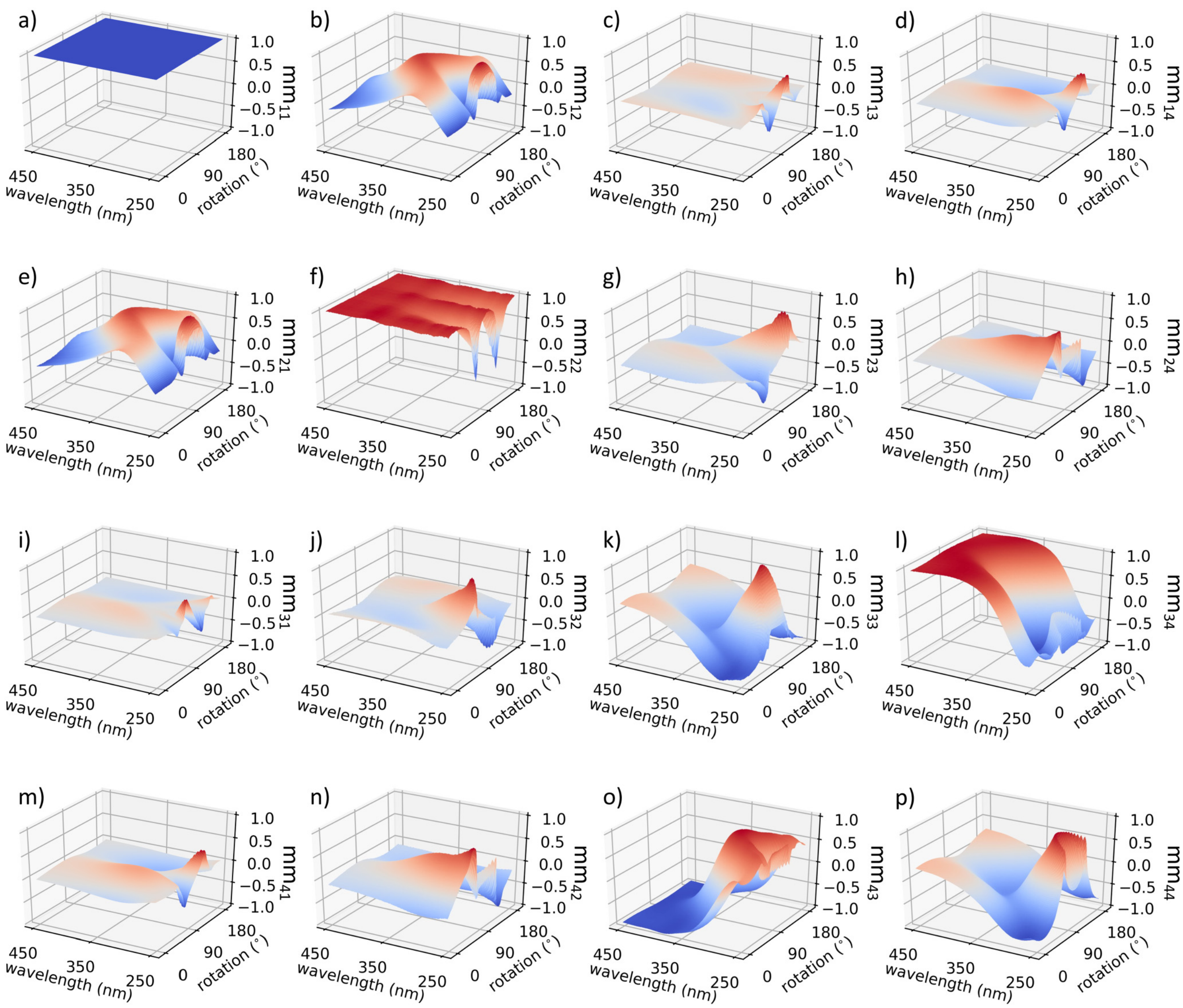

FIG. 5. Normalized Mueller matrix measured under different azimuthal rotations of sample A with an angle of incidence of 75°. Each graph shows an element of the normalized Mueller matrix measured at different wavelengths and different azimuthal rotation angles (corresponding to the two horizontal axes of the individual figures). The 16 graphs correspond to the 16 MM elements as defined in Eqs. (3) and (4).

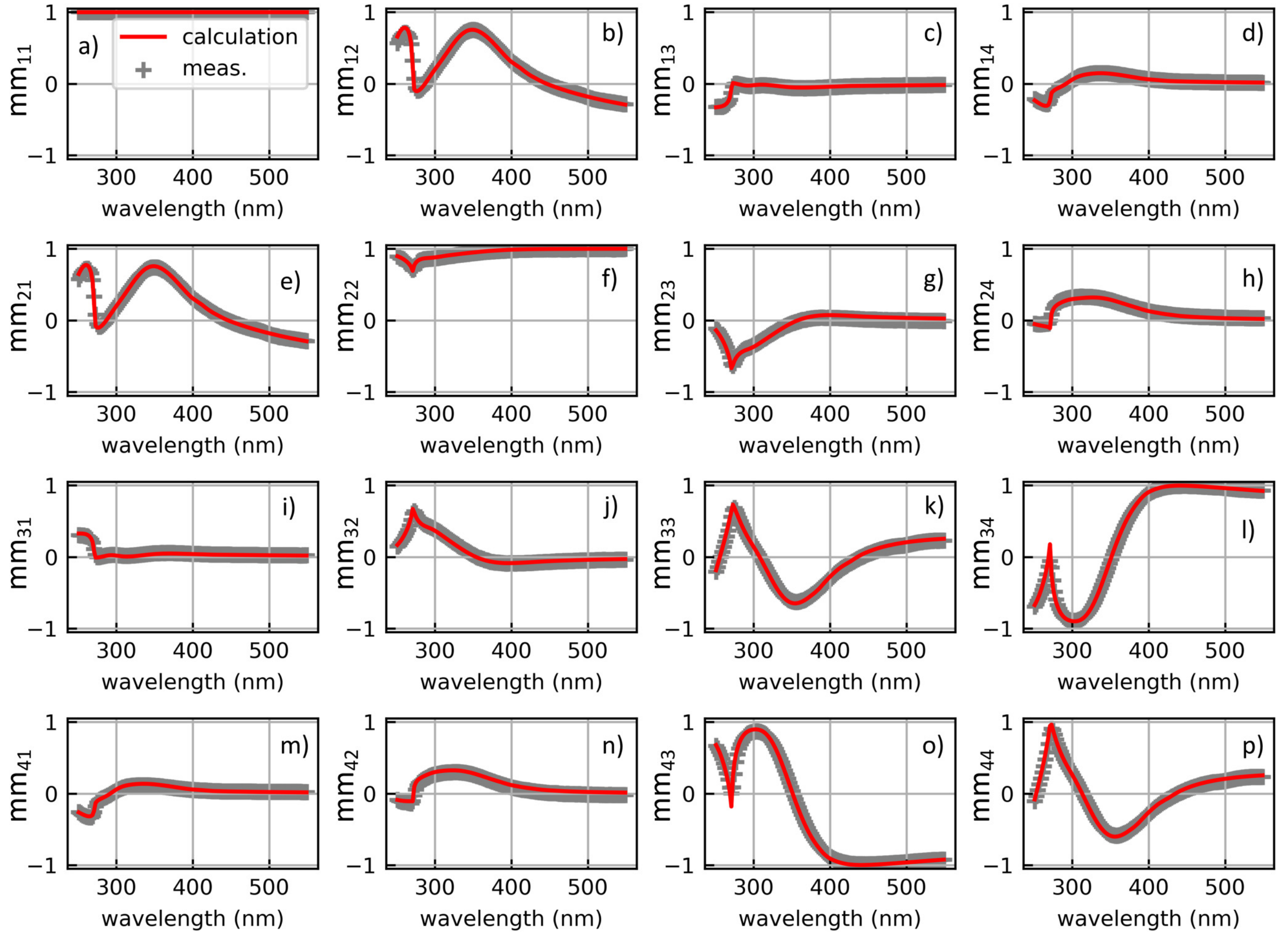

FIG. 6. Normalized Mueller-matrix measurement and model calculation results of sample A with an angle of incidence of 75° measured at an azimuthal angle of 90° in the same coordinate system as in Figs. 4 and 5. The 16 graphs correspond to the 16 MM elements as defined in Eqs. (3) and (4).

orientation, as shown in Fig. 4, where the measured Δ values at $\lambda = 290$ nm are plotted as a function of azimuthal rotation angle for sample A. Finding the grating orientation is then reduced to finding the extremum of a curve.

This turns out to be a reliable detection method, which does not require any modeling effort. This method, however, may not be reliable when the grating period does not support any of Wood's resonances, or the signatures of the resonances are too weak or too numerous to analyze without an accurate physical model. Another disadvantage is the definite need for the specific azimuthal rotation hardware to be included in the measurement apparatus.

B. MM-MBD measurement of samples

In recent years, significant effort has been made to use MM-SE measurements in periodic structure characterization metrologies, and it has been shown that this method can be superior in many ways when compared to simpler SE-based metrologies. It enables the characterization of structure asymmetries, like fin-bending[13,18] and even line edge roughness.[19] In our example, we present the most basic of such asymmetries, the tilting in the orientation of the grating lines.

Rotating the samples in the azimuthal direction and measuring the MM show clear signs of the orientation of the anisotropic properties of the sample, as seen in Fig. 5. At the rotation angle where the grating lines are either perpendicular to or parallel with the plane of incidence, the 2 by 2 submatrices located on top right and bottom left of the full MM become zero. Notice in Eq. (4) that these elements become exactly zero, when the cross-terms r_{ps} and r_{sp} are both zero.

At this orientation, the measured MM contains little additional information about the sample compared to the standard SE measurements. However, even in this case, the zero elements of MM provide an additional check of the grating line orientation. At other orientations, the additional information provided by the MM measurements makes it possible to deduce asymmetries in the structures or trench profiles, in our example, the orientation of the grating lines. In the following part, we show results from a single MM measurement, without using the data from the azimuthal rotation of the sample to illustrate the advantage of MM-MBD metrology.

Sample A evaluated with the MM-MBD method measured shows a grating line orientation angle of around 105°, the same value as found by multiple SE-MBD measurements with the azimuthal rotation of the sample. In Fig. 6, the results of the measured and calculated MM are plotted, showing

TABLE III. MM-MBD and AFM results for sample A. Grating angle is an additional fitting parameter in MM-MBD measurement. Static repeatability was found to be better than 0.32% (1 sigma) for all values except the residual thickness, in which case it is 0.55%.

	Grating angle (deg)	Pitch (nm)	Residual thickness (nm)	Grid depth (nm)	MCD (nm)
MM-MBD	105.6	143.6	21.3	90.3	61.3
AFM	—	141.9	—	89.6	80.3

good agreement for all components of the matrix. The fitted structure parameters and residual layer thickness are also very similar when compared to SE-MBD and AFM measurements of the sample as summarized in Table III. In this case, the azimuthal angle is an additional (the sixth) floating parameter.

In this case, the fitting algorithm and the model calculation are significantly more time-consuming, owing to the extra fitting parameter (azimuthal angle) and to the necessity of modeling the structure in conical incidence. In this case, the computation effort can be the main factor limiting the time-to-solution, i.e., the time needed to measure the sample and evaluate the measurement data. The offline generation of a data library prior to the measurement can significantly reduce the time to solution. At conical incidence the measured SE quantities also depend on the cross-terms in Eq. (2). Therefore, even if the orientation of the grating lines is known prior to the measurement, the computation time of the full MM is essentially the same as computing only SE quantities in such grid line orientations.

It should be noted that the measurement of the 15-element Mueller matrix requires a more complex optical hardware with two compensators (or photoelastic modulators). In the dual compensator configuration, one of the compensators is rotating, and the other one is either stepping or continuously rotating.[9] Dual rotating compensators can also be realized by using two M-Prisms as compensating elements.[20] In the case of a dual rotating compensator configuration, there is no additional time required to measure the normalized MM as compared to the only measuring Ψ and Δ. With the corresponding hardware and computational capability, MM-MBD metrology can characterize gratings with an uncertain grating angle orientation accurately and quickly. On the other hand, if the grating line orientation is determined from multiple measurements of the sample, a more complex mechanical hardware is required, and the modeling and fitting procedure may be even more computationally demanding, because the sample has to be modeled in multiple optical configurations in conical incidence.

The clear advantage of the MM-MBD method is the accurate characterization of structure parameters even if there is uncertainty in the grating line orientation. This enables the characterization of additional structure parameters (in our case, the azimuthal angle) with comparable precision, without the definite need of additional mechanical hardware complexity or multiple measurements. Thus, the MM-MBD method can detect and characterize structure parameters and the grating line angle from a single measurement.

V. SUMMARY AND CONCLUSIONS

In summary, we have compared methods of periodic structure characterization based on spectral ellipsometry and Mueller-matrix spectral ellipsometry for the characterization of 1D gratings with uncertain grating orientation. Nanoimprinted GaAs wafers from the preproduction line of VCSEL devices were used as test samples, with 1D periodic gratings formed in the GaAs substrate and SiO_2 coating. We compared the two methods in terms of measurement and modeling difficulties and shown that the MM-MBD metrology can produce accurate results from a single measurement even if the orientation of the grating line is uncertain. The results of the characterization methods were validated by AFM measurements of the samples.

ACKNOWLEDGMENTS

The authors are grateful to I. Kükemezei and G. László for validating the results with additional AFM measurements. They are grateful to Ö. Sepsi for valuable discussions and ideas on the RCWA models and L. Szabó for software development.

[1] K. J. Ebeling, R. Michalzik, and H. Moench, Jpn. J. Appl. Phys. **57**, 08PA02 (2018).
[2] M. Grabherr, R. King, R. Jäger, D. Wiedenmann, P. Gerlach, D. Duckeck, and C. Wimmer, Proc. Soc. Photo-Opt. Instrum. **6908**, 690803 (2008).
[3] K. Iga, Jpn. J. Appl. Phys. **47**, 1 (2008).
[4] R. Michalzik, *VCSELs, Fundamentals, Technology and Applications of Vertical-Cavity Surface-Emitting Lasers*, Springer Series in Optical Sciences (Springer, Berlin, 2013).
[5] T. Ohtoshi, T. Kuroda, A. Niwa, and S. Tsuji, Appl. Phys. Lett. **65**, 1886 (1994).
[6] P. Debernardi and G. P. Bava, IEEE J. Sel. Top. Quantum Electron. **9**, 905 (2003).
[7] M. A. Verschuuren, P. Gerlach, H. A. van Sprang, and A. Polman, Nanotechnology **22**, 505201 (2011).
[8] H. Fujiwara, *Spectroscopic Ellipsometry Principles and Applications* (Wiley, Chichester, 2007).
[9] H. G. Tompkins and E. A. Irene, *Handbook of Ellipsometry* (William Andrew, Norwich, 2005).
[10] S. Enoch and N. Bonod, *Plasmonics: From Basics to Advanced Topics*, Springer Series in Optical Sciences Vol. 167 (Springer, Berlin, 2012).
[11] A. A. Darweesh, S. J. Bauman, D. T. Debu, and J. B. Herzog, Nanomaterials **8**, 809 (2018).
[12] X. Chen, C. Zhang, and S. Liu, Appl. Phys. Lett. **103**, 151605 (2013).
[13] X. Chen, C. Zhang, S. Liu, H. Jiang, Z. Ma, and Z. Xu, J. Appl. Phys. **116**, 194305 (2014).
[14] M. G. Moharam and T. K. Gaylord, J. Opt. Soc. Am. **71**, 811 (1981).
[15] M. G. Moharam, E. B. Grann, D. A. Pommet, and T. K. Gaylord, J. Opt. Soc. Am. A **12**, 1068 (1995).
[16] M. G. Moharam, D. A. Pommet, E. B. Grann, and T. K. Gaylord, J. Opt. Soc. Am. A **12**, 1077 (1995).
[17] B. Dhoedt, "Theoretical and experimental study of free-space optical interconnections based on diffractive lens arrays," Ph.D. thesis (Ghent University, 1995).
[18] A. C. Diebold, A. Antonelli, and N. Keller, APL Mater. **6**, 058201 (2018).
[19] D. Dixit *et al.*, J. Micro Nanolithogr. MEMS MOEMS **14**, 031208 (2015).
[20] L. Makai, Hungarian patent P1900183 (May 2019).